



# In situ Growth and Characterization of Lubricious Carbon-Based Films Using Colloidal Probe Microscopy

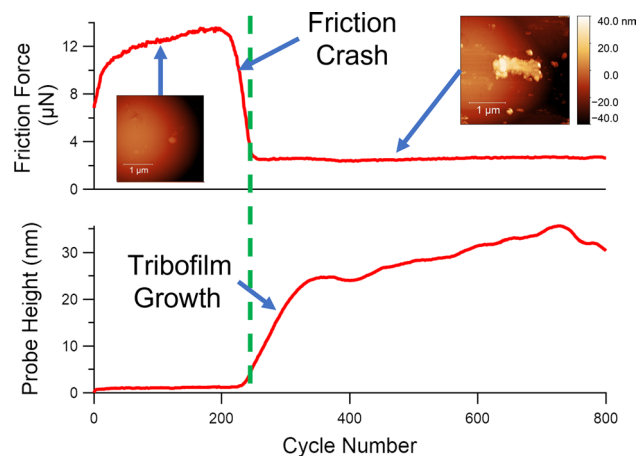
J. Brandon McClimon<sup>1</sup> · James Hilbert<sup>1</sup> · Komlavi Dzidula Koshigan<sup>2</sup> · Julien Fontaine<sup>2</sup> · Jennifer R. Lukes<sup>1</sup> · Robert W. Carpick<sup>1</sup>

Received: 11 January 2023 / Accepted: 14 February 2023 / Published online: 1 March 2023  
© The Author(s), under exclusive licence to Springer Science+Business Media, LLC, part of Springer Nature 2023

## Abstract

Silicon oxide-doped hydrogenated amorphous carbon (a-C:H:Si:O) is an important form of diamond-like carbon (DLC) for tribological applications, primarily because of its enhanced thermal stability and reduced dependence of friction on environmental humidity. As with other DLCs, its mechanisms of lubrication are still an active area of research, though it is now known that surface passivation and tribofilm growth are important factors. In this study, tribofilm formation for a-C:H:Si:O is examined at the microscale by using steel colloid atomic force microscopy probes as the sliding counterface. This approach provides some inherent advantages over macroscale tribology experiments, namely that the tribofilm thickness and stiffness can be tracked in situ and correlated directly with the friction response. The results of these experiments show that the tribofilm grows rapidly on the steel colloid following a period of counterface wear and high friction. The friction drops more than 80% upon nucleation of the tribofilm, which is attributed to a decrease of more than 80% in adhesion combined with a decrease in the estimated interfacial shear strength of at least 65%. Approximately 80% of the friction decrease occurs before the tribofilm reaches a thickness of 2 nm, suggesting that only the near-surface properties of the tribofilm provide the needed functionality for its effective lubrication mechanisms.

## Graphical abstract



**Keywords** DLC · Tribofilm · Silicon and oxygen-containing hydrogenated amorphous carbon (a-C:Si:O) · Colloidal probe microscopy

✉ Robert W. Carpick  
carpick@seas.upenn.edu

Extended author information available on the last page of the article

## 1 Introduction

Diamond-like Carbons (DLC) are an important class of materials for tribology applications [1–3], among many others [4–6]. These protective coatings simultaneously provide low or even superlubric ( $\mu < 0.01$ ) friction coefficients, [7] and very low wear, which is an uncommon and valuable combination. As such, understanding their lubrication mechanisms is important for further development of DLC materials for tribological applications. Effort has been devoted to achieving this understanding for decades [8]. At this point, the importance of a surface passivation mechanism is well-established [9–16], where passivating species from the environment or dopants, especially –H and –OH groups, terminate dangling bonds at the DLC surface thereby preventing the formation of interfacial bonds to the countersurface which lead to high friction and wear. In addition, a second mechanism, the formation of a counterface tribofilm (sometimes referred to as a transfer film), has also been identified as important in the lubrication performance of DLCs [7, 17–20]. Studies of tribofilm composition and structure in a-C:H:Si:O films similar to those examined here are relatively less common than in Si-free DLC's, but our prior characterization shows that the tribofilm is segregated into C-rich and Si-rich domains [18], and hence, it reasonable to posit that the C-rich domains have similar structure and lubrication mechanisms as tribofilms grown from Si-free DLCs. The importance of tribofilms in DLC sliding experiments was recognized by the early 1990s [21], when macroscale tribology experiments showed that the presence of the tribofilm on the stainless steel counterface was a necessary condition for low friction and wear. Various spectroscopies, including Raman, X-ray photoelectron (XPS), and electron energy loss (EELS), have been utilized to understand the structure and composition of DLC-derived tribofilms. Such studies have determined that the tribofilms are typically enriched in hydrogen [6, 7, 18], suggesting that surface passivation of the tribofilm may contribute to lubricity in a similar fashion to the DLC counterface. Additionally, a substantial fraction of  $sp^3$ -bonded carbon is sometimes present [7, 18]. Nanoindentation experiments have found low elastic moduli and hardness values along with substantial viscoelasticity of DLC-derived tribofilms [18], which suggests that the tribofilms may be polymeric in nature. How or whether such a structure might contribute to lubricity is not understood at present.

This work focuses on the formation of tribofilm in a DLC system using a microscale contact. The specific system is a silicon oxide-doped hydrogenated amorphous carbon (a-C:H:Si:O) which has been characterized spectroscopically [22], and studied in nanoscale [23] and macroscale [18] sliding experiments. In macroscale tribometer experiments

of a steel ball sliding against a-C:H:Si:O, stable tribofilms formed readily and low friction coefficients ( $\mu = 0.05$ – $0.2$ ) were observed. In contrast, in the nanoscale experiments with an a-C:H:Si:O counterface, tribofilm formation typically did not occur, and very high interfacial shear strengths (1–10 GPa) were found in both dry and humid sliding environments.

Microscale contact sizes represent an intermediate lengthscale. At first glance, it is not obvious why one should interrogate this lengthscale. The contact geometry is similar to that found at the macroscale, composed of at least hundreds of individual asperities, each of which should exhibit a tribological response similar to what is found in AFM experiments. This geometry also generally forecloses the possibility of using contact mechanics to understand the evolution of important parameters such as real contact area and local stress distributions near the interface. There are several advantages to working at this lengthscale, however. The tests to be discussed were performed with smooth colloidal AFM probes ( $< 0.5$  nm RMS). The use of spherical colloids allows for expansion of the possible counterface chemistries and structures relative to sharp AFM probes, where one is typically limited to a few materials such as Si, diamond, and DLC. Lower contact pressures can also be achieved relative to AFM studies with sharp tips due to the reduced dominance of adhesion on the total normal pressure, thus broadening the range of pressures studied. [23] Additionally, wear of the probe has a less dramatic effect on the contact geometry in the case of colloidal probes. The use of an AFM for testing opens up the possibility of making measurements that are difficult or impossible at the macroscale, such as the level of adhesion or the characterization of counterface morphology *in situ*. One can also use modulation techniques such as measuring the normal stiffness of the contact during the test [24], which provides insight into the mechanical properties of the sliding contact.

The tribology of DLC has been examined at the microscale in the past [25–28]. Several studies utilized nanoindentation equipment to perform scratch testing, where the sharp nanoindentation probe is dragged along the DLC surface with a controlled normal load and, sometimes, resolution of the resulting lateral forces [29–32]. The wear tracks from such tests can also be characterized *in situ* in some cases. These tests are especially useful for characterizing the quality of adhesion between thin films and their substrates. Understanding this adhesion has been critical for the hard drive industry to develop protective overcoats for their magnetic media, and so there has been significant work in this area. The extreme conditions during these tests are also useful for characterizing the wear resistance of the coatings themselves. In some cases, nanoindenters have been used to perform reciprocating sliding and thereby examine layer-by-layer removal of coating materials. [33] As with standard

AFM, the availability of only a few tip materials is a major limitation.

Using colloidal AFM probes to study the tribological response of DLC as we do here is rare in the literature. In one case, colloidal AFM was used to evaluate the effect of micropatterning and ionic liquid lubrication on DLC microtribological response using a polystyrene ball [34]. The lateral forces were uncalibrated, so only relative friction performance between the various DLCs could be evaluated. The linear rise of friction with normal load also indicated that the contact maintained a multi-asperity contact geometry. In another study, a very close analog to the experiments which will be presented was run, involving steel colloidal probes sliding on another a-C:H:Si:O [11]. In these tests, the macroscale run-in effect was observed, as well as a similar dependence of friction on environment. It was concluded, based on post-test imaging, that the formation of the tribofilm was responsible for the run-in effect.

## 2 Experimental Methodology

All experiments were conducted in an RHK 350 AFM (RHK Technology, Troy, MI) housed in an environmentally controlled chamber and controlled by an RHK R9 controller. Steel colloids with composition and mechanical properties close to those of 52100 bearing steel with a nominal diameter of 40  $\mu\text{m}$  (SHS7574HV1, NanoSteel Company, Inc., Providence, RI, USA) were glued onto tapping mode cantilevers (NCHR, NanoWorld AG, Neuchâtel, Switzerland) using epoxy (JB Weld, JB Weld Company, Atlanta, GA, USA). The colloid apex geometry, which can vary substantially from the nominal diameter, was characterized by inverse imaging using tapping mode of an array of oxide-sharpened silicon spikes (the same shape that is used in popular sharp Si AFM tips) with apex radii nominally below 10 nm (TGT1, NT-MDT Spectrum Instruments, Moscow, Russia) [35]. This provides topographic information about the colloid probe, distorted by only a small amount due to convolution with the sharp silicon probe. The colloid radius was determined by fitting a circle to the linescans across at least three such reverse images of the TGT1 sample spikes. Tip-sample convolution effects were neglected given the much larger radius of the colloids relative to the TGT spike apices. These images were also used for colloid roughness determination. The local RMS roughness of the colloid was  $<0.5$  nm across the maximum nominal contact area of the tests presented here (approximately  $220 \times 220$  nm<sup>2</sup>). Normal forces were calibrated using the reference cantilever method yielding normal spring constants of 20–40 N/m for the various cantilevers used [36]. Lateral forces were calibrated using the diamagnetic lateral force calibration method [37]. Sliding tests were performed on an a-C:H:Si:O film

custom-grown by NCD Technologies (Madison, WI) on a Si wafer using the plasma immersion ion implantation and deposition method from a hexamethyldisiloxane precursor, as described previously [22]. The bulk composition of the 40-nm-thick a-C:H:Si:O film was  $26 \pm 10$  at.% carbon,  $11 \pm 5$  at.% silicon,  $15 \pm 4$  at.% oxygen,  $47 \pm 4$  at.% hydrogen as determined by Rutherford backscattering spectroscopy and forward recoil elastic scattering, with an  $\text{sp}^3$  C fraction of  $73 \pm 3$  at.% measured by near edge X-ray absorption fine structure spectroscopy. [18] The RMS roughness of the a-C:H:Si:O was 0.16 nm across  $1 \times 1$   $\mu\text{m}^2$ , as measured with AFM [22]. AFM measurements were conducted in either dry nitrogen ( $<5\%$  RH) or humid nitrogen ( $50 \pm 5\%$  RH), controlled by continuous flow of nitrogen from the boil-off of a liquid nitrogen dewar, with some fraction bubbled through deionized water to provide humidity when needed.

High load (1–3  $\mu\text{N}$ ) reciprocating sliding tests were conducted across 2  $\mu\text{m}$  sliding tracks at a speed of 4  $\mu\text{m}/\text{s}$  in  $50 \pm 5\%$  RH  $\text{N}_2$  while applying a sinusoidal oscillation of 50 pm amplitude at 3 kHz to the Z-piezo to capture the normal stiffness of the system. A high humidity was chosen for the tribofilm growth because earlier macroscale experiments in the same material system led to stiffer tribofilms that adhered better to a steel counterface. [18] Similar tribofilms in this microscale system were judged as more likely to survive in situ characterization with the AFM probe. In that case, the contact was a multi-asperity contact, which was known from the load chosen and the local roughness parameters determined from AFM imaging of the bare colloid. [38] The Z-oscillation frequency was chosen to be above the low-pass filter cutoff of 2 kHz for the feedback circuitry; thus, the normal force topographic feedback was unaffected by the imposed Z-oscillation. The normal force signal was fed into a lock-in amplifier using the Z-oscillation signal as a reference, so that the lock-in output provided the force response to the oscillation signal. This technique is referred to as force modulation microscopy (FMM) [39].

Friction as a function of load was measured at a sliding speed of 3  $\mu\text{m}/\text{s}$  across a  $5 \times 5$   $\mu\text{m}^2$  region with a constant increase in the normal load after each of 128 scan lines. The large transverse spatial increment between scan lines (5  $\mu\text{m}/128$  lines = 39 nm) was chosen to minimize wear of the a-C:H:Si:O, and therefore, also the dependence of friction on wear-induced changes to the a-C:H:Si:O. It also served to minimize any additional growth of the tribofilm. Each measurement was immediately repeated with a decreasing load to verify repeatability and to capture the load range between pull-in and pull-off which occurred at a negative applied load due to adhesive forces between the a-C:H:Si:O and steel probe.

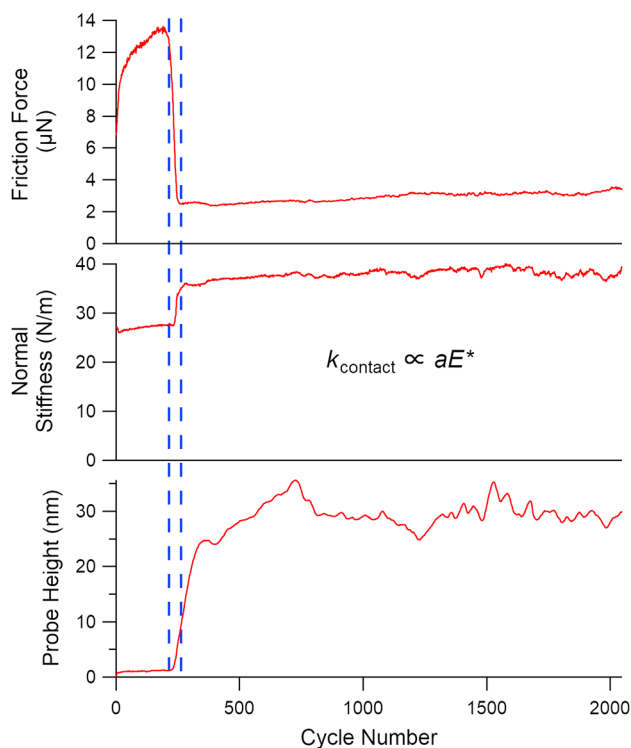


**Fig. 1** Friction force, total normal stiffness, and probe height acquired simultaneously during reciprocating sliding at  $4 \mu\text{m/s}$  across a  $2 \mu\text{m}$  wear track of a steel colloid on a-C:H:Si:O with a  $2.9 \mu\text{N}$  normal load in the humid  $\text{N}_2$  environment. Cycle number refers to the number of reciprocating sliding cycles since the start of the test. A  $3 \text{ kHz}$  Z-oscillation of  $50 \text{ pm}$  amplitude was applied during the test, which allowed for tracking of the normal stiffness and phase, which measures the composite stiffness of both the cantilever and the contact. The generalized relationship between contact stiffness, real area of contact, and reduced modulus is shown. A close up of the transition zone marked in blue is provided in Figure S1

### 3 Results

The primary goal of this study was to grow a tribofilm in situ. To achieve this, the steel colloid probe of apex radius  $50 \mu\text{m}$  was subjected to reciprocating sliding at an applied normal load of  $2.9 \mu\text{N}$  across a scan length of  $2 \mu\text{m}$ . With an adhesion force of  $735 \text{ nN}$  determined via the pull-off force measurement, a Derjaguin–Müller–Toporov (DMT) [40] estimate of the maximum normal contact pressure and contact radius were  $120 \text{ MPa}$  and  $120 \text{ nm}$ , respectively. It should be noted that since this is a multi-asperity contact, as will be shown later, there are asperities which will experience higher normal stresses and the real area of contact will be much smaller than the DMT contact radius would imply.

Figure 1 shows the evolution of the friction force, the total normal stiffness, and probe height obtained from topography data, acquired simultaneously, during the reciprocating sliding test. The total normal stiffness is shown, which depends on both the cantilever and contact stiffness. Since

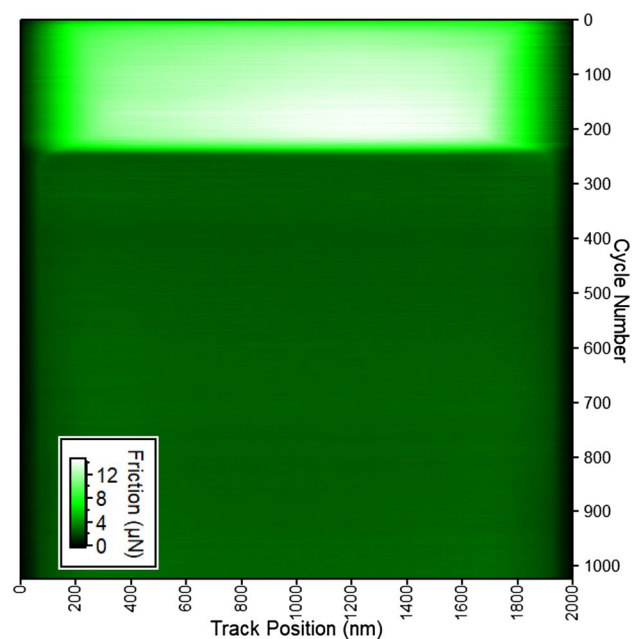


**Fig. 2** Friction force as a function of sliding cycles during reciprocating sliding of the steel colloid on a-C:H:Si:O in  $50\% \text{RH } \text{N}_2$  with a  $2.9 \mu\text{N}$  load. Horizontal features correspond to changes in time, vertical features, if present, would indicate changes to particular wear track regions

the cantilever stiffness is constant throughout the test, any changes are due to variations in the normal contact stiffness. From cycle 1 through approximately cycle 200, the friction doubles and the total stiffness increases by approximately 7%. The probe height increases by  $1.2 \text{ nm}$ . At least a fraction of this change is due to downward creep of the Z-piezo after the initial transient of applying the normal load, [41] which the feedback circuit compensates for. This creep effect also compensates for any wear of the a-C:H:Si:O or ball, which would otherwise lead to some decrease in the measured tip height. Two plausible explanations for the friction increase are that asperities are being removed from both counterfaces, thus increasing the true contact area, and/or the oxide layer is being removed from the steel, thus exposing the more adhesive and reactive bare steel, which exhibits a higher shear strength. The former would lead to an increase in the real contact area, which increases the normal stiffness and friction. The latter would increase friction due to increased shear strength. In addition, more adhesion and greater contact area would increase formation of adhesive junctions [42] with the exposed bare steel. If an oxide was removed, one would expect a decrease in the topographic height. However, the initial piezo creep effect may obscure such a change.

Starting at cycle 210, the friction begins to drop precipitously before the normal stiffness jumps and the topographic height begins to increase at cycle 225, while the friction continues to decrease. This is clear evidence of the



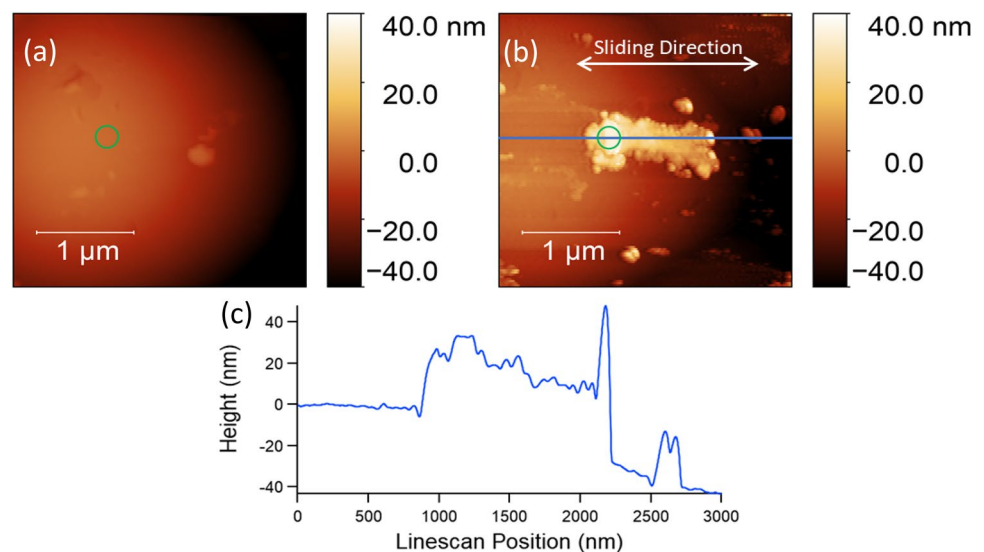
nucleation and growth of a tribofilm. This process occurs during approximately 120 cycles, whereupon the friction has dropped by 81%, the normal stiffness increases by 30%, and the probe height increases by  $25 \pm 2$  nm (a close up of this transition region marked in blue is provided in Figure S1.). The topography/probe height signal change is due to the probe being lifted by the feedback circuit to maintain a constant normal load, consistent with the growth of a tribofilm on the probe. Simultaneous wear of the sample or ball which would reduce the height increase is judged to be small, given the stability of the topography signal for the prior 200 cycles. The increase in the normal stiffness indicates that the real contact area grows substantially if the assumption is made that the tribofilm possesses similar mechanical properties as those grown at macroscale, [18] since it was found in that macroscale study that the tribofilms had much lower average elastic moduli than the initial counterfaces. Thus, a change in only the mechanical properties of the material at the contact should reduce the normal stiffness; the increase seen here can thus only be explained if the contact area increases. That friction is primarily controlled by the tribofilm formation is also supported by the friction image (sometimes referred to as a triboscopy map [43]) in Fig. 2, which is constant across the wear track (except at the left and right edges where the effect of static friction produces an artificial apparent low friction force). If friction was primarily controlled by changes to the a-C:H:Si:O, one would expect a friction dependence on position in the wear track (i.e., one would see vertical features in the image shown in Fig. 2), unless such changes occur homogeneously across the wear track. It should be noted, however, that 24.5% of the total friction decrease occurs prior to any detectable change in the probe height, suggesting that chemical and structural

changes at the counterface surfaces drive a significant fraction of the friction reduction.

For the remainder of the test, the changes are less dramatic. The topography continues to grow before saturating at a value of  $28.4 \pm 2.3$  nm, suggesting the tribofilm grows to this thickness level and then roughly maintains a steady-state thickness. Notably, the friction is approximately constant during this growth, indicating that the friction reduction is primarily controlled by the chemistry and structure of the tribofilm near the a-C:H:Si:O/tribofilm interface, and not by the overall thickness of the tribofilm. Post-sliding imaging did not reveal any transfer of tribofilm back to the a-C:H:Si:O. There is a slow increase in the friction and normal stiffness, 27% and 8%, respectively, throughout the remainder of the test. These results can be explained by some additional growth in the real contact area as the tribofilm grows in lateral extent due to plastic deformation and/or material transport/shearing of the tribofilm.

It should be noted here that the implied friction coefficients are very high relative to what is typically seen at macroscale, in the presence or absence of tribofilm. Prior to tribofilm formation, the friction coefficient is  $> 4$ , and after the tribofilm formation remains above 0.9. At the macroscale, on this sample in this environment, with a similar steel counterface, the friction coefficient was  $< 0.16$ . [18] This disparity can be rationalized, in part, by considering that non-Amontonian friction has been observed in macroscale studies on DLC after formation of the lubricating tribofilm, so that the concept of a friction coefficient lacks validity in this system. This power law friction scaling (seen here as well, see below) has been used to estimate the interfacial shear strength in macroscale DLC contacts. [44] Assuming Hertzian scaling holds for simplicity, the friction coefficient should scale with  $R^{2/3}/F^{2/3}$  where  $R$  is the ball radius and  $F$  is the applied load. Under that assumption, a reduction in

**Fig. 3** **a** Topographic contact-mode AFM image of steel colloid prior to reciprocating sliding test. **b** Topographic tapping-mode image of colloid after the reciprocating sliding test at 2.9  $\mu\text{N}$  applied load shown in Figs. 1 and 2. Green circles represent nominal contact area determined from DMT contact mechanics for bare a-C:H:Si:O/steel. **(c)** Linescan from **(b)**



the ball radius and applied normal load to match the microscale experiment here would increase the friction coefficient found in Ref. 18 to 0.32. This does not match the friction coefficient of 0.9 found here, but as we will show, there is evidence to suggest the formation of the tribofilm leads to a growth in the nominal contact area beyond the initial Hertzian contact diameter, which might account for the disparity.

Figure 3 shows pre- and post-test reverse imaging of the colloidal probe using a TGT1 sample. The post-test measurement was done in tapping mode rather than contact mode to minimize wear of the tribofilm. It is clear from the linescan shown in Fig. 3c that the thickness of the tribofilm ( $33.6 \pm 8.8$  nm) agrees reasonably well with the  $28.4 \pm 2.3$  nm which was measured during the sliding test, with the difference likely reflecting compression of the tribofilm due to the normal load during the wear test. In fact, a very rough estimate of the Young's modulus can be made by treating the colloid as a cylindrical punch of radius equal to the DMT contact radius of the original a-C:H:Si:O-steel contact, and also making the more reasonable assumption of incompressible DLC and steel, to yield a value of 517 MPa. This value represents an upper bound, given that we can see in Fig. 3b that the tribofilm diameter far exceeds the DMT prediction, thus the contact area used in the modulus calculation is an underestimate. Note that the tribofilms grown in macroscale sliding experiments also showed much smaller elastic moduli relative to the starting a-C:H:Si:O which had an elastic modulus of 120 GPa [18].

The tribofilm is elongated in the sliding direction. Since torsion of the cantilever during the two sliding directions of the probe changes the real area of contact for each direction, it might explain elongation of the tribofilm in the sliding direction. However, the magnitude of such an expected change can be estimated from the static friction at the track endpoints in, e.g., Fig. 2, to be approximately 200 nm total. This is not large enough to explain the magnitude of the elongation. The fact that the tribofilm appears to have formed at an offset from the colloid apex (with the center of the tribofilm approximately  $1.5 \mu\text{m}$  to the right of the center of the probe) may be due to an experimental artifact. The topography was measured by scanning the colloid over a spiked TGT1 sample. A difference in the slope of TGT1 sample relative to the a-C:H:Si:O sample under the probe of as little as  $2^\circ$  could produce the offset seen here. It is also possible poor adhesion between the tribofilm and steel allowed it to slide. The presence of wear debris above and below the apex in Fig. 3b outside the horizontal band containing the tribofilm suggests the tribofilm may have moved from where it was originally grown. Prior literature has shown that tribofilm adhesion to steel counterfaces can be poor, depending on tribofilm growth conditions. [45–47]

The wide lateral extent of the tribofilm in all directions relative to the nominal contact area requires explanation. In

the macroscale work [18], where a similar effect was seen for sliding in a flowing  $\text{N}_2$  environment, we attributed this effect to a combination of plastic deformation and viscoelastic flow due to the soft polymeric properties of the tribofilm, which were found to have highly laterally inhomogeneous hardness values of  $300 \pm 320$  MPa in Ref. 18. Flow out of the contact area may help explain the self-termination of the vertical growth of the tribofilm, with extra tribofilm volume beyond the thickness where the tribofilm is stable being shed out of the contact area and increasing the lateral extent of the tribofilm. An additional piece of evidence that material flow is a relevant mechanism is that in our prior characterization of macroscale a-C:H:Si:O tribofilms [18], we found that the tribofilm was organized into a segregated Si-rich and C-rich domain structure with individual domains spanning hundreds of nm. Gross material flow is a possible mechanism for achieving such segregation, although selective adhesive transfer of Si atoms to Si-rich and C atoms to C-rich domains is another possible mechanism that could lead to this domain structure.

An additional possibility, given that the thickness of these tribofilms is a significant fraction of the nominal contact radius, is that the nominal contact area increases because of a decrease in the reduced Young's Modulus  $E^*$  of the contact due to the formation of the soft tribofilm itself. In the macroscale work, it was found that all regions of tribofilms grown in a humid environment had elastic moduli  $< 40$  GPa, at least a 60% reduction relative to the bearing steel on which they were grown, with many areas exhibiting orders of magnitude smaller elastic moduli. Since the nominal contact area in DMT contact mechanics scales with  $E^{*-2/3}$ , a 50% reduction in  $E^*$  for example leads to a 58% increase in the nominal contact area. Thus, a large reduction in  $E^*$  due

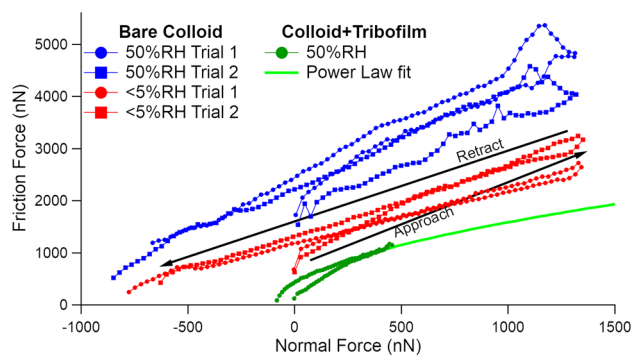


**Fig. 4** Friction vs. applied normal load for a steel colloid sliding on a-C:H:Si:O with or without a tribofilm in multiple environments. Tests were performed by approaching via increasing load setpoint, then retracting to pulloff, as indicated by arrows. The presented tribofilm test was performed in 50%RH  $\text{N}_2$ . Black arrows illustrate the test progression from pull in during the approach to pull off during retraction

to tribofilm growth can produce a substantial increase in the nominal area of contact.

To examine the tribological response of the steel colloid sliding on a-C:H:Si:O, with and without the tribofilm, a series of friction vs. load measurements were performed. In the bare colloid tests, humid and dry environments were examined. For the colloid-with-tribofilm tests, a smaller load range was used to minimize damage to the tribofilm. Tests were performed in multiple environments (see SI Fig S2), but it was apparent that the tribofilm was evolving throughout these tests, so only the first is presented here, where the tribofilm geometry and structure had not yet changed significantly. This test was performed in the same humid environment in which it was grown (50% RH). All tests were performed on pristine (previously unscanned) regions of the a-C:H:Si:O sample. Note that the maximum load reached, 1.35  $\mu\text{N}$ , is significantly less than the 2.9  $\mu\text{N}$  load used previously to generate a tribofilm on a bare colloid probe.

Results are presented in Fig. 4. Focusing on the bare colloid results, it is clear that there is a strong humidity dependence to the friction. The nearly linear dependence of friction on load is consistent with a multi-asperity contact geometry [48]. The magnitude and slope of the linear dependence are higher in the humid case. Such a humidity dependence was absent in the case of the tribofilm + colloid trials. The humidity dependence in the bare colloid case might be due in part to capillary adhesion. While steel can have large water contact angles suggesting a high surface energy, [49] this is influenced by the presence of surface oxides and organic contamination, [50] which can be removed from the contact zone by sliding. The underlying metal will have a high surface energy [51] and tend to form substantial capillary bridges in a humid environment.

The friction vs. load measurement with a tribofilm present on the colloid shows several distinct, important features. First, the adhesion (the pull-off force reached during retraction) is reduced by at least 80%: 29 nN is obtained, vs. 775 nN and 849 nN for the humid and dry bare colloid cases, respectively. This is remarkable considering the increase in real contact area upon tribofilm growth, to be discussed below. The reduction in adhesion results in reduced friction across the entire load range, relative to the bare colloid results, shifting the friction vs. load curve to the right. The idea that there has been a change from a patchy, multi-asperity contact to a more continuous area of contact is supported by a power law fit to the contact area vs. load (Fig. 4), where the scaling exponent was 0.52. If we assume a constant shear strength [52], the expected scaling exponent for a perfect, single-asperity DMT contact is  $2/3$ , as opposed to the case of a multi-asperity contact which obeys Amontons's law, where the scaling exponent would be 1 (as was seen for the bare colloid). This very low scaling exponent indicates the contact is behaving as a single asperity contact. The fact that the

exponent is lower than the lower bound of the range between single and multi-asperity contacts is not fully understood, but may have to do with the fact that the tribofilm is not spherical in shape, but rather more like a flat plateau. In such cases, the contact area would grow more slowly with normal load than would be the case for a spherical contact [53]. This can be understood by considering the extreme case of a rigid, flat punch. Friction vs. load curves in such a case (again assuming constant shear strength) would result in a scaling exponent of 0 since the real contact area does not grow with load.

## 4 Discussion

The compilation of results presented here provides important insight about the fundamental lubrication mechanisms for steel and perhaps other materials sliding on a-C:H:Si:O. The reciprocating sliding testing presented in Fig. 1 represents the clearest evidence to date that the growth of a tribofilm on the steel counterface is the primary mechanism leading to low friction in a DLC material. By monitoring friction, stiffness, and height simultaneously, it was possible to detect tribofilm and correlate its nucleation to the moment the drop in friction occurs. The closest prior results have come to accomplishing this for DLC is studies that have used an optical camera focused through a transparent counterface to detect when a tribofilm was present in macroscale sliding experiments either visually or with Raman spectroscopy [54, 55], although it has been recognized frequently in the past that the formation of a tribofilm, usually observed *ex situ* after testing is completed, is correlated with large reductions in friction [42].

The technique presented here offers additional insights. The termination of the friction reduction after the tribofilm has grown  $< 5$  nm in thickness indicates that there is little dependence of the friction on the thickness of the tribofilm beyond a small threshold value. As Figure S1 shows, 80% of the friction reduction occurs before the tribofilm reaches a thickness of 2 nm. This result indicates that it is important for researchers to use surface-sensitive spectroscopy to confirm or refute the presence of a tribofilm before making conclusions about what is driving friction reduction in DLC tribology experiments. It also suggests the relevant system size to understand the lubricity is small enough that molecular dynamics simulations could be a useful tool, if the tribofilm's composition and structure can be well-determined.

It was also noted that 24.5% of the total friction decrease occurs before any measurable ( $\pm 0.2$  nm resolution) probe height change occurs. This suggests a surface effect drives some fraction of the friction reduction. Prior literature offers guidance for interpreting this result, with a surface enrichment of passivating species [6, 10, 12] and structural

changes to the DLC near-surface region such as carbon ring orientation changes [56] as defensible explanations. A related explanation supported by the data here is that a reduction in adhesion might cause some of this early friction reduction, given that a large adhesion change occurred upon growth of the tribofilm. Such an adhesion reduction would reduce friction levels, although we cannot say with confidence how much of the adhesion reduction occurs prior to the tribofilm growing to a substantial thickness. The triboscopy map in Fig. 2 shows that even during this initial stage of friction reduction, the changes are uniform across the wear track, so changes cannot be unambiguously attributed to changes on the DLC side of the counterface. It should also not be assumed that these near-surface effects are responsible for 24.5% of the shear strength reduction, since the normal stiffness data show that the real area in contact grows substantially after this initial friction decrease is complete.

One can use these data to gain insight about what is occurring during the friction drop. From the topography trace in Fig. 1, the friction reduction occurs during the initial 5 nm of tribofilm growth (see Figure S1 for zoomed version). We use DMT contact mechanics to estimate when contact between the steel and the a-C:H:Si:O is completely lost during growth of the tribofilm. Based on the applied normal load, mechanical properties of the colloid and a-C:H:Si:O, radius of the colloid, and pre-sliding adhesion value, we calculated the normal deformation of the steel colloid due to the applied normal load, which is  $< 0.2$  nm during the experiment. While asperities may deflect more than this due to higher local contact pressures, the overall roughness of the colloid near the apex is  $< 0.5$  nm, so lifting the steel colloid 1–2 nm should be more than sufficient to eliminate all direct contact between the steel and the a-C:H:Si:O. Therefore, the friction continues to drop after the steel colloid has lost all direct contact with the a-C:H:Si:O. This suggests that there is some dependence of the shear strength on the tribofilm thickness across a small range of thickness values, apparently up to 5 nm in thickness.

The results present evidence that there is a very large increase in the real area of contact as the tribofilm grows. First, the increase in stiffness despite the growth of a low modulus tribofilm demonstrates an increase in contact area. Based on the earlier estimate of  $< 1$  GPa for the tribofilm elastic modulus, the stiffness increase during tribofilm growth implies that the real contact area grows by more than 100x. Second, the change from linear scaling to power law scaling after the growth of tribofilm in the friction vs. load curves demonstrates that the real area of contact is much larger in the tribofilm case. Finally, the direct post-test imaging of the colloid in Fig. 3b shows that the lateral extent of the tribofilm far exceeds the diameter expected from DMT contact mechanics.

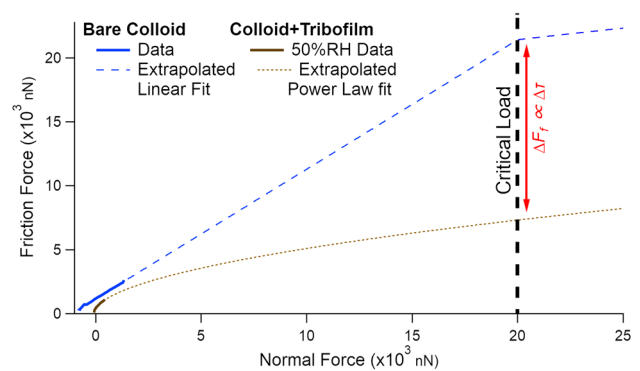


**Fig. 5** Extrapolation of data fits in Fig. 4 to the critical load where a single-asperity contact geometry is expected to be achieved for the bare colloid case. From the extrapolation, the interfacial shear strength reduction due to the tribofilm formation can be estimated

Since we know the real area of contact is much larger when the tribofilm is present, we can also conclude, based on the disparity in friction at a given load between the bare colloid and the colloid with the tribofilm, that the formation of the tribofilm is accompanied by a large drop in the interfacial shear strength. As the load grows, the difference in friction also grows between the tribofilm and bare colloid cases, as seen in Fig. 4. At some point, upon increasing the load further, the bare colloid will compress enough asperities such that the real contact area is nearly equal to the nominal contact area, and the bare colloid friction will change from linear scaling with load to power law scaling consistent with single asperity contact mechanics. This critical load, 20  $\mu$ N, was estimated from the mechanical properties of the counterfaces and a roughness parameter of the colloid, which we know from AFM imaging of the colloid surface, using the model of Pastewka and Robbins for the elastic contact of a sphere with self-affine surface roughness on a flat surface [38]. At this critical load, the real areas of contact for the bare colloid and the colloid + tribofilm should be nearly equal, aside from the growth of the tribofilm beyond the initial nominal contact area. This allows for an estimate of the minimum reduction in interfacial shear strength upon growth of the tribofilm. This will be an underestimate because we know from post-sliding imaging (Fig. 3b) that the tribofilm grows laterally beyond the initial nominal contact area. Extrapolating the curves displayed in Fig. 4 for the bare colloid  $< 5\%$  RH Trial 1 and the colloid with the tribofilm measurement to this critical load (Fig. 5), one finds that there is a 65% difference in the extrapolated friction, and therefore, we posit that at least a 65% reduction in the interfacial shear strength exists. Given the scale of lateral tribofilm growth beyond the initial nominal contact area, the real reduction in the shear strength is likely much larger. It should be emphasized that this reduction in shear strength is much greater than what was found for the



nanoscale run-in effect for hard asperity contacts discussed in our previous work, where tribofilm was absent [23]. By contrast, another recent study using sharp AFM probes to slide on a highly hydrogenated a-C:H in ultrahigh vacuum did manage to nucleate and grow tribofilms on the probe, which led to very large friction reductions. In that case, they present convincing evidence that true graphitization of the tribofilm was likely the source of the tribofilm's lubricity. [57]

The humidity-dependent friction vs. load measurements for the colloid with the tribofilm, shown in Figure S2, demonstrated that there was little detectable dependence on the humidity. This was unexpected, given a universally strong dependence in macroscale sliding experiments. One possible explanation is that these experiments do not present a sufficiently accurate analog to macroscale experiments, where the humidity dependence has been shown on worn films, whereas these friction vs. load measurements were done on unworn a-C:H:Si:O.

## 5 Conclusions

In this study, it has been shown via sliding experiments of a steel colloid on an a-C:H:Si:O film using an AFM that a tribofilm can be grown at the microscale with in situ detection of its growth and a simultaneous drop in the friction. The drop in the friction is attributed to two primary effects. The first is an 80% reduction in adhesion, which reduces the friction at any given applied load. The second is a reduction in the interfacial shear strength. The experimental data are comprehensive enough that a lower bound estimate of the fractional reduction in interfacial shear strength can be made, which shows that the shear strength is reduced by at least 65%. The formation of the tribofilm is accompanied by a large increase in the real area of contact, which would lead to an increase in friction if the adhesion and shear strength remained constant. Instead, the reductions in adhesion and shear strength lead to an overall reduction in friction, with the degree of friction reduction increasing at higher applied loads.

The results presented here provide new mechanistic understanding of how a tribofilm allows for a low friction interface, even though a full atomically-resolved explanation requires further work. The most useful result to guide future understanding and optimization of these types of coatings is that only the near-surface layer (essentially the top 2 nm) contributes to friction reduction. As such, the structural features leading to the friction reduction are likely to be accessible with near-surface spectroscopies such X-ray photoelectron spectroscopy and near-edge X-ray absorption spectroscopy. Molecular dynamics simulations could also be a valuable tool, much as they have

been for understanding DLC lubrication mechanisms in the absence of a tribofilm. Two nm of material in the vertical direction is a computationally tractable system size, although knowledge of the specific structure and composition of this region is still required.

Across such a limited thickness range, existing work may be worth considering. For instance, the heavily studied class of self-assembled monolayers and their mechanisms of friction reduction may be relevant if the near-surface of the tribofilm is predominantly composed of linear chains. Unfortunately, structural details beyond composition and carbon hybridization state remain unknown and should be a focus of future study. This work also suggests paths to further optimization of tribological properties. For instance, if only the near-surface of the tribofilm contributes to friction reduction, growth of the tribofilm to larger thicknesses is undesirable in that it leads to an increase in the real area of contact, which increases the overall friction force the contact. Likewise, a comprehensive understanding of the tribofilm structure could allow for rationally-designed ultrathin tribological coatings for demanding applications like MEMS where reductions in both adhesion and shear strength would be useful.

**Supplementary Information** The online version contains supplementary material available at <https://doi.org/10.1007/s11249-023-01712-9>.

**Acknowledgements** This material is based upon work supported by the Advanced Storage Technology Consortium ASTC (Grant 2011-012), the National Science Foundation under Grant No. DMR-1107642, the National Science Foundation through the University of Pennsylvania Materials Research Science and Engineering Center (MRSEC) (DMR-1720530), and by the Agence Nationale de la Recherche under Grant No. ANR-11- NS09-01 through the Materials World Network program. NSF Major Research Instrumentation Grant DMR-0923245 and use of the Scanning and Local Probe Facility of the Singh Center for Nanotechnology, which is supported by the NSF National Nanotechnology Coordinated Infrastructure Program under grant NNCI-2025608, are acknowledged.

**Author contributions** JBM conceived and performed the experiments and wrote the manuscript. JH helped conceive and perform the experiments. KMK conceived and performed the experiments. JF conceived and supervised the experiments. JL conceived and supervised the experiments. RWC conceived and supervised the experiments.

**Funding** Advanced Storage Technology Consortium, 2011-012, National Science Foundation, DMR-1720530 and NNCI-2025608, Agence Nationale de la Recherche, ANR-11- NS09-01.

**Data Availability** All data utilized for the manuscript and supplemental information is available upon request from the corresponding author.

## Declarations

**Competing interests** The authors declare no competing interests.

## References

- Arnoldussen, T.C., Rossi, E.-M.: Materials for magnetic recording. *Annu. Rev. Mater. Sci.* **15**, 379–409 (1985). <https://doi.org/10.1146/annurev.ms.15.080185.002115>
- Erdemir, A., Donnet, C.: Tribology of diamond-like carbon films: recent progress and future prospects. *J. Phys. D: Appl. Phys.* **39**, R311 (2006). <https://doi.org/10.1088/0022-3727/39/18/R01>
- Vetter, J.: 60years of DLC coatings: historical highlights and technical review of cathodic arc processes to synthesize various DLC types, and their evolution for industrial applications. *Surf. Coat. Technol.* **257**, 213–240 (2014). <https://doi.org/10.1016/j.surfcoat.2014.08.017>
- Casiraghi, C., Robertson, J., Ferrari, A.C.: Diamond-like carbon for data and beer storage. *Mater. Today* **10**, 44–53 (2007). [https://doi.org/10.1016/S1369-7021\(06\)71791-6](https://doi.org/10.1016/S1369-7021(06)71791-6)
- Petersen, M., Heckmann, U., Bandorf, R., Gwozdz, V., Schnabel, S., Bräuer, G., Klages, C.-P.: Me-DLC films as material for highly sensitive temperature compensated strain gauges. *Diam. Relat. Mater.* **20**, 814–818 (2011). <https://doi.org/10.1016/j.diamond.2011.03.036>
- Mangolini, F., Krick, B.A., Jacobs, T.D.B., Khanal, S.R., Streller, F., McClimon, J.B., Hilbert, J., Prasad, S.V., Scharf, T.W., Ohlhausen, J.A., Lukes, J.R., Sawyer, W.G., Carpick, R.W.: Effect of silicon and oxygen dopants on the stability of hydrogenated amorphous carbon under harsh environmental conditions. *Carbon* **130**, 127–136 (2018). <https://doi.org/10.1016/j.carbon.2017.12.096>
- Chen, X., Zhang, C., Kato, T., Yang, X., Wu, S., Wang, R., Nosaka, M., Luo, J.: Evolution of tribo-induced interfacial nanostructures governing superlubricity in a-C: H and a-C:H: Si films. *Nat. Commun.* **8**, 1675 (2017). <https://doi.org/10.1038/s41467-017-01717-8>
- Oguri, K., Arai, T.: Low friction coatings of diamond-like carbon with silicon prepared by plasma-assisted chemical vapor deposition. *J. Mater. Res.* **5**, 2567–2571 (1990). <https://doi.org/10.1557/JMR.1990.2567>
- Cui, L., Lu, Z., Wang, L.: Environmental effect on the load-dependent friction behavior of a diamond-like carbon film. *Tribol. Int.* **82**, 195–199 (2015). <https://doi.org/10.1016/j.triboint.2014.10.014>
- Konicek, A.R.: Influence of surface passivation on the friction and wear behavior of ultrananocrystalline diamond and tetrahedral amorphous carbon thin films. *Phys. Rev. B.* (2012). <https://doi.org/10.1103/PhysRevB.85.155448>
- Koshigan, K.D.: Understanding the influence of environment on the solid lubrication processes of carbon-based thin films. *Ecully, Ecole centrale de Lyon* (2015)
- Romero, P.A., Pastewka, L., Lautz, J.V., Moseler, M.: Surface passivation and boundary lubrication of self-mated tetrahedral amorphous carbon asperities under extreme tribological conditions. *Friction* **2**, 193–208 (2014). <https://doi.org/10.1007/s40544-014-0057-z>
- Chen, Y.-N., Ma, T.-B., Chen, Z., Hu, Y.-Z., Wang, H.: Combined effects of structural transformation and hydrogen passivation on the frictional behaviors of hydrogenated amorphous carbon films. *J. Phys. Chem. C.* **119**, 16148–16155 (2015). <https://doi.org/10.1021/acs.jpcc.5b04533>
- Donnet, C., Fontaine, J., Grill, A., Mogne, T.L.: The role of hydrogen on the friction mechanism of diamond-like carbon films. *Tribol. Lett.* **9**, 137–142 (2001). <https://doi.org/10.1023/A:1018800719806>
- De Barrosouchet, M.-I., Zilibotti, G., Matta, C., Righi, M.C., Vandenbulcke, L., Vacher, B., Martin, J.-M.: Friction of diamond in the presence of water vapor and hydrogen gas. Coupling gas-phase lubrication and first-principles studies. *J. Phys. Chem. C.* **116**, 6966–6972 (2012). <https://doi.org/10.1021/jp211322s>
- Koshigan, K.D., Mangolini, F., McClimon, J.B., Vacher, B., Bec, S., Carpick, R.W., Fontaine, J.: Understanding the hydrogen and oxygen gas pressure dependence of the tribological properties of silicon oxide-doped hydrogenated amorphous carbon coatings. *Carbon* **93**, 851–860 (2015). <https://doi.org/10.1016/j.carbon.2015.06.004>
- Manimunda, P., Al-Azizi, A., Kim, S.H., Chromik, R.R.: Shear-Induced Structural Changes and Origin of Ultralow Friction of Hydrogenated Diamond-like Carbon (DLC) in Dry Environment. *ACS Appl. Mater. Interfaces.* **9**, 16704–16714 (2017). <https://doi.org/10.1021/acsami.7b03360>
- McClimon, J.B., Lang, A.C., Milne, Z., Garabedian, N., Moore, A.C., Hilbert, J., Mangolini, F., Lukes, J.R., Burris, D.L., Taheri, M.L., Fontaine, J., Carpick, R.W.: Investigation of the mechanics, composition, and functional behavior of thick tribofilms formed from silicon- and oxygen-containing hydrogenated amorphous carbon. *Tribol Lett.* **67**, 48 (2019). <https://doi.org/10.1007/s11249-019-1155-x>
- Singer, I.L., Dvorak, S.D., Wahl, K.J., Scharf, T.W.: Role of third bodies in friction and wear of protective coatings. *J. Vac. Sci. Technol., A* **21**, S232–S240 (2003). <https://doi.org/10.1116/1.1599869>
- Godet, M.: Third-bodies in tribology. *Wear* **136**, 29–45 (1990). [https://doi.org/10.1016/0043-1648\(90\)90070-Q](https://doi.org/10.1016/0043-1648(90)90070-Q)
- Sugimoto, I., Miyake, S.: Oriented hydrocarbons transferred from a high performance lubricative amorphous C:H: Si film during sliding in a vacuum. *Appl. Phys. Lett.* **56**, 1868–1870 (1990). <https://doi.org/10.1063/1.103072>
- Mangolini, F., McClimon, J.B., Segersten, J., Hilbert, J., Heaney, P., Lukes, J.R., Carpick, R.W.: Silicon oxide-rich diamond-like carbon: a conformal, ultrasmooth thin film material with high thermo-oxidative stability. *Adv. Mater. Interfaces* **6**, 1801416 (2019). <https://doi.org/10.1002/admi.201801416>
- McClimon, J.B., Hilbert, J., Lukes, J.R., Carpick, R.W.: Nanoscale run-in of silicon oxide-doped hydrogenated amorphous carbon: dependence of interfacial shear strength on sliding length and humidity. *Tribol Lett.* **68**, 80 (2020). <https://doi.org/10.1007/s11249-020-01319-4>
- Carpick, R.W., Ogletree, D.F., Salmeron, M.: Lateral stiffness: a new nanomechanical measurement for the determination of shear strengths with friction force microscopy. *Appl. Phys. Lett.* **70**, 1548–1550 (1997). <https://doi.org/10.1063/1.118639>
- Chung, K.-H., Kim, D.-E.: Fundamental investigation of micro wear rate using an atomic force microscope. *Tribol. Lett.* **15**, 135–144 (2003). <https://doi.org/10.1023/A:1024457132574>
- Bhushan, B., Koinkar, V.N.: Nanoindentation hardness measurements using atomic force microscopy. *Appl. Phys. Lett.* **64**, 1653–1655 (1994). <https://doi.org/10.1063/1.111949>
- Wiens, A., Persch-Schuy, G., Vogelgesang, M., Hartmann, U.: Scratching resistance of diamond-like carbon coatings in the subnanometer regime. *Appl. Phys. Lett.* **75**, 1077–1079 (1999). <https://doi.org/10.1063/1.124602>
- Ferrari, A.C.: Diamond-like carbon for magnetic storage disks. *Surf. Coat. Technol.* **180–181**, 190–206 (2004). <https://doi.org/10.1016/j.surfcoat.2003.10.146>
- Czyzniewski, A.: Optimising deposition parameters of W-DLC coatings for tool materials of high speed steel and cemented

- carbide. *Vacuum* **86**, 2140–2147 (2012). <https://doi.org/10.1016/j.vacuum.2012.06.011>
30. Fukui, H., Irie, M., Utsumi, Y., Oda, K., Ohara, H.: An investigation of the wear track on DLC (a-C:H) film by time-of-flight secondary ion mass spectroscopy. *Surf. Coat. Technol.* **146–147**, 378–383 (2001). [https://doi.org/10.1016/S0257-8972\(01\)01422-0](https://doi.org/10.1016/S0257-8972(01)01422-0)
  31. Neerincx, D., Persoone, P., Sercu, M., Goel, A., Kester, D., Bray, D.: Diamond-like nanocomposite coatings (a-C:H/a-Si:O) for tribological applications. *Diam. Relat. Mater.* **7**, 468–471 (1998). [https://doi.org/10.1016/S0925-9635\(97\)00201-X](https://doi.org/10.1016/S0925-9635(97)00201-X)
  32. Tsai, P.-C., Hwang, Y.-F., Chiang, J.-Y., Chen, W.-J.: The effects of deposition parameters on the structure and properties of titanium-containing DLC films synthesized by cathodic arc plasma evaporation. *Surf. Coat. Technol.* **202**, 5350–5355 (2008). <https://doi.org/10.1016/j.surfcoat.2008.06.073>
  33. Poirié, T., Schmitt, T., Bousser, E., Martinu, L., Klemberg-Sapieha, J.E.: In situ real time nanowear testing method of optical functional thin films. *Tribol. Int.* **95**, 147–155 (2016). <https://doi.org/10.1016/j.triboint.2015.10.020>
  34. Zhao, W., Pu, J., Yu, Q., Zeng, Z., Wu, X., Xue, Q.: A Novel strategy to enhance micro/nano-tribological properties of DLC film by combining micro-pattern and thin ionic liquids film. *Colloids Surf., A* **428**, 70–78 (2013). <https://doi.org/10.1016/j.colsurfa.2013.03.047>
  35. Nalam, P.C., Gosvami, N.N., Caporizzo, M.A., Composto, R.J., Carpick, R.W.: Nano-rheology of hydrogels using direct drive force modulation atomic force microscopy. *Soft Matter* **11**, 8165–8178 (2015). <https://doi.org/10.1039/C5SM01143D>
  36. Cook, S.M., Schäffer, T.E., Chynoweth, K.M., Wigton, M., Simmonds, R.W., Lang, K.M.: Practical implementation of dynamic methods for measuring atomic force microscope cantilever spring constants. *Nanotechnology* **17**, 2135 (2006). <https://doi.org/10.1088/0957-4484/17/9/010>
  37. Li, Q., Kim, K.-S., Rydberg, A.: Lateral force calibration of an atomic force microscope with a diamagnetic levitation spring system. *Rev. Sci. Instrum.* **77**, 065105 (2006). <https://doi.org/10.1063/1.2209953>
  38. Pastewka, L., Robbins, M.O.: Contact area of rough spheres: Large scale simulations and simple scaling laws. *Appl. Phys. Lett.* **108**, 221601 (2016). <https://doi.org/10.1063/1.4950802>
  39. Radmacher, M., Tillmann, R.W., Gaub, H.E.: Imaging viscoelasticity by force modulation with the atomic force microscope. *Biophys. J.* **64**, 735–742 (1993). [https://doi.org/10.1016/S0006-3495\(93\)81433-4](https://doi.org/10.1016/S0006-3495(93)81433-4)
  40. Derjaguin, B.V., Muller, V.M., Toporov, Yu.P.: Effect of contact deformations on the adhesion of particles. *J. Colloid Interface Sci.* **53**, 314–326 (1975). [https://doi.org/10.1016/0021-9797\(75\)90018-1](https://doi.org/10.1016/0021-9797(75)90018-1)
  41. Jung, H., Gweon, D.-G.: Creep characteristics of piezoelectric actuators. *Rev. Sci. Instrum.* **71**, 1896–1900 (2000). <https://doi.org/10.1063/1.1150559>
  42. Fontaine, J., Le Mogne, T., Loubet, J.L., Belin, M.: Achieving superlow friction with hydrogenated amorphous carbon: some key requirements. *Thin Solid Films* **482**, 99–108 (2005). <https://doi.org/10.1016/j.tsf.2004.11.126>
  43. dos Santos, M.B., Costa, H.L., De Mello, J.D.B.: Potentiality of triboscopy to monitor friction and wear. *Wear* **332–333**, 1134–1144 (2015). <https://doi.org/10.1016/j.wear.2014.10.017>
  44. Scharf, T.W., Ohlhausen, J.A., Tallant, D.R., Prasad, S.V.: Mechanisms of friction in diamondlike nanocomposite coatings. *J. Appl. Phys.* (2007). <https://doi.org/10.1063/1.2711147>
  45. Hauert, R.: An overview on the tribological behavior of diamond-like carbon in technical and medical applications. *Tribol. Int.* **37**, 991–1003 (2004). <https://doi.org/10.1016/j.triboint.2004.07.017>
  46. Ronkainen, H., Koskinen, J., Likonen, J., Varjus, S., Vihersalo, J.: Characterization of wear surfaces in dry sliding of steel and alumina on hydrogenated and hydrogen-free carbon films. *Diam. Relat. Mater.* **3**, 1329–1336 (1994). [https://doi.org/10.1016/0925-9635\(94\)90147-3](https://doi.org/10.1016/0925-9635(94)90147-3)
  47. Ronkainen, H., Likonen, J., Koskinen, J., Varjus, S.: Effect of tribofilm formation on the tribological performance of hydrogenated carbon coatings. *Surf. Coat. Technol.* **79**, 87–94 (1996). [https://doi.org/10.1016/0257-8972\(95\)02433-6](https://doi.org/10.1016/0257-8972(95)02433-6)
  48. Greenwood, J.A., Williamson, J.B.P.: Contact of nominally flat surfaces. *Proc. R. Soc. Lond. Ser. A* **295**, 300–319 (1966). <https://doi.org/10.1098/rspa.1966.0242>
  49. Kalin, M., Polajnar, M.: The wetting of steel, DLC coatings, ceramics and polymers with oils and water: the importance and correlations of surface energy, surface tension, contact angle and spreading. *Appl. Surf. Sci.* **293**, 97–108 (2014). <https://doi.org/10.1016/j.apsusc.2013.12.109>
  50. Mantel, M., Wightman, J.P.: Influence of the surface chemistry on the wettability of stainless steel. *Surf. Interface Anal.* **21**, 595–605 (1994). <https://doi.org/10.1002/sia.740210902>
  51. Tyson, W.R., Miller, W.A.: Surface free energies of solid metals: Estimation from liquid surface tension measurements. *Surf. Sci.* **62**, 267–276 (1977). [https://doi.org/10.1016/0039-6028\(77\)90442-3](https://doi.org/10.1016/0039-6028(77)90442-3)
  52. Carpick, R.W., Ogletree, D.F., Salmeron, M.: A general equation for fitting contact area and friction vs load measurements. *J. Colloid Interface Sci.* **211**, 395–400 (1999). <https://doi.org/10.1006/jcis.1998.6027>
  53. Carpick, R.W., Agraït, N., Ogletree, D.F., Salmeron, M.: Measurement of interfacial shear (friction) with an ultrahigh vacuum atomic force microscope. *J. Vacuum Sci. Technol. B* **14**, 1289–1295 (1996). <https://doi.org/10.1116/1.589083>
  54. Scharf, T.W., Singer, I.L.: Monitoring transfer films and friction instabilities with in situ raman tribometry. *Tribol. Lett.* **14**, 3–8 (2003). <https://doi.org/10.1023/A:1021942830132>
  55. Scharf, T.W., Singer, I.L.: Role of third bodies in friction behavior of diamond-like nanocomposite coatings studied by in situ tribometry. *Tribol. Trans.* **45**, 363–371 (2002). <https://doi.org/10.1080/10402000208982561>
  56. Ma, T.-B., Wang, L.-F., Hu, Y.-Z., Li, X., Wang, H.: A shear localization mechanism for lubricity of amorphous carbon materials. *Sci. Rep.* (2014). <https://doi.org/10.1038/srep03662>
  57. Wang, K., Zhang, J., Ma, T., Liu, Y., Song, A., Chen, X., Hu, Y., Carpick, R.W., Luo, J.: Unraveling the friction evolution mechanism of diamond-like carbon film during nanoscale running-in process toward superlubricity. *Small* **17**, 2005607 (2021). <https://doi.org/10.1002/sml.202005607>

**Publisher's Note** Springer Nature remains neutral with regard to jurisdictional claims in published maps and institutional affiliations.

Springer Nature or its licensor (e.g. a society or other partner) holds exclusive rights to this article under a publishing agreement with the author(s) or other rightsholder(s); author self-archiving of the accepted manuscript version of this article is solely governed by the terms of such publishing agreement and applicable law.

## Authors and Affiliations

J. Brandon McClimon<sup>1</sup> · James Hilbert<sup>1</sup> · Komlavi Dzidula Koshigan<sup>2</sup> · Julien Fontaine<sup>2</sup> · Jennifer R. Lukes<sup>1</sup> · Robert W. Carpick<sup>1</sup>

<sup>1</sup> Department of Mechanical Engineering & Applied Mechanics, University of Pennsylvania, 220 South 33rd Street, Philadelphia, PA, USA

<sup>2</sup> Laboratoire de Tribologie Et Dynamique Des Systèmes LTDS, UMR CNRS 5513, Université de Lyon, Ecole Centrale de Lyon, 36 Avenue Guy de Collongue, 69134 Ecully, France